

All-polymer-based ammonia gas sensor: applying insights from the morphology-driven ac electrical performance

Ana Carolina Kelmer¹ , Cleidinéia Cavalcante da Costa^{2*}  and Rodrigo Fernando Bianchi² 

¹*Courage and Khazaka Electronic, Cologne, Germany*

²*Laboratório de Polímeros e de Propriedades Eletrônicas de Materiais, Departamento de Física, Universidade Federal de Ouro Preto – UFOP, Ouro Preto, MG, Brasil*

*cleidineiasm@gmail.com

Abstract

This paper investigates the electrical, morphological, and mechanical behavior of ultrathin layer-by-layer polyaniline/poly(vinyl sulfonic acid) (PANI/PVS) ultrathin films for ammonia gas sensing. Atomic force microscopy shows that the PANI/PVS surface's roughness increases almost linearly with the number of PANI/PVS bilayers, while the surface morphology varies from a rod-like structure to a film-like architecture. Impedance measurements and their representation by a Cole-Cole model confirm this transition at ~15 bilayers. The designed sensor shows low response time (< 1 min), an optimal operating frequency range (1–100 Hz), high stability and sensibility to ammonia (~ 98 kΩ/ppm), and low sensibility to strain (~ 3.6 kΩ/%). This study suggests that hopping carriers' concentration remains constant, and hopping carriers' mobility changes with the number of bilayers. The simultaneous analysis of morphology with complex impedance measurements is a strategy for enhancing the electrical performance of low-cost and flexible organic sensing devices.

Keywords: *conductivity, printed devices, sensing devices, strain gauges, topology.*

How to cite: Kelmer, A. C., Costa, C. C., & Bianchi, R. F. (2024). All-polymer-based ammonia gas sensor: applying insights from the morphology-driven ac electrical performance. *Polímeros: Ciência e Tecnologia*, 34(1), e20240012. <https://doi.org/10.1590/0104-1428.20230070>

1. Introduction

There has been substantial interest in the manufacture of flexible electronic materials and device innovations, including flexible displays^[1], wearable health monitoring^[2], and gas detection technologies^[3]. Furthermore, conjugated polymers have attracted the attention of industries due to their excellent characteristics for sensing applications, such as the possibility of tuning chemical and physical properties using different substituents, as mentioned in the literature review^[4]. However, this field's main challenge is still achieving high-performance devices with ultra-sensitive detection, fast response, low consumption, reproducibility, easy fabrication, mechanical and electrical stabilities, and good portability and flexibility^[5-8]. In fact, a comprehensive understanding of the physical principles underlying surface morphology, electrical behavior, and mechanical properties are desired for the design of high-performance flexible devices using solution-processable components on flexible substrates^[9-13]. This is the case for polyaniline (PANI)-based devices used to detect harmful gases which response depends on the type (dc or ac) electrical measurements to characterize the gas under examination^[13-20]. This situation leads to measurement-to-measurement variations^[21,22]. Many studies have focused on the electrical field frequency-dependent impedance characteristics of ultrathin semiconducting polymer-based sensors as a practical solution to avoid sensor instability effects^[13,23-27].

This paper highlights the importance of simultaneously exploring the morphology and complex impedance measurements

to provide a powerful methodology for enhancing the electrical performance of promising polymer-based flexible ultrathin films for sensor technology development.

2. Materials and Methods

2.1 Ultrathin layer-by-layer (LBL) films

Ultrathin layer-by-layer (LBL) films formed by alternating layers of positively charged PANI and negatively charged poly(vinyl sulfonic acid) (PVS) were prepared on flexible polystyrene (PS) substrate (thickness of ~200 μm and area of ~600 mm²) according to the procedures described by Santos et al.^[26] PANI/PVS adsorption was monitored by ultraviolet-visible (UV-Vis) spectroscopy with a Shimadzu UV-1650PC spectrophotometer. Finally, an estimation for a single PANI/PVS bilayer thickness, ~ (4 ± 1) nm, was obtained by measuring the thickness of a 40 bilayers film using a DekTak 6 M Stylus Profiler from Veeco Instruments Inc. More details can be found in our previous paper^[26]. The morphological surface properties of the PANI/PVS/PS films were studied by atomic force microscopy (AFM, Park System XE7-Series SPM Controller) operating in non-contact mode with NSC35/Al BS cantilevers, which allowed us to characterize the surface of the bilayers on the flexible (i.e. polystyrene) substrate. More details of AFM image analysis can be found in our previous paper^[28].

2.2 PANI/PVS ammonia gas sensor results

Figure 1 shows a schematic illustration of the fabrication process of semiconducting polymer PANI/PVS-based flexible devices. The ultrathin LBL films were obtained by alternating layers of positively charged PANI and negatively charged PVS on flexible PS using the same procedure described by Santos et al.^[26] shown in Figure 1a. Figure 1b shows the representation of the PANI/PVS films on the PS substrate. A parallel pair of solution-processed silver electrodes (thickness of $\sim 3 \mu\text{m}$) on the PANI/PVS surface was obtained from a screen-printing technique that uses CI-1001 ECM silver ink and a screen mask (polyester stencil screen) with well-defined windows, as shown in Figure 1c. A mechanical cutting process (Figure 1d) was used to establish single sensors (Figure 1e). An image of the ammonia gas sensors using PANI/PVS films on the PS substrate is shown in Figure 1f.

2.3 Electrical characterization

Complex impedance measurements, $Z^*(f) = Z'(f) - iZ''(f)$, of the PANI/PVS sensors, were carried out using a 1260 Solartron frequency response analyzer in the 1 to 106 Hz frequency range, with a voltage amplitude equal to 1.5 V. All electrical measurements were carried out in a homemade gas chamber at room temperature. More details can be found in^[26,27,29]. The ammonia-air mixture was injected into the chamber at a 1 ppm/min rate, which was continuously recorded during the electrical measurements using a high-performance electrochemical diffusion ammonia sensor (Instrutherm DG-200). Uniaxial tensile experiments were carried out for mechanical testing using an EMIC DL2000 Universal Testing Machine from 0 to 250 N (or 0 to 25% strain) with a 500 kgf load cell and simultaneously

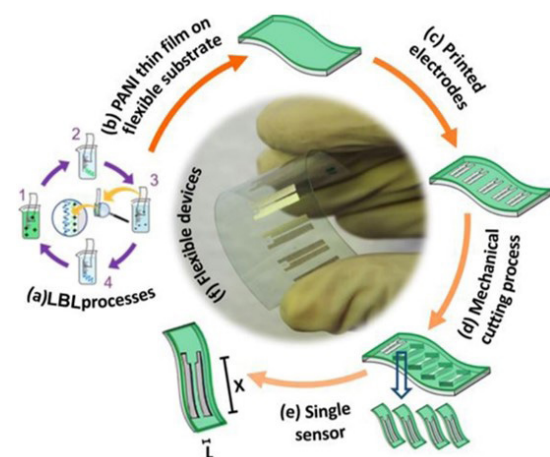


Figure 1. Schematic illustration of the fabrication process of the PANI/PVS-based flexible devices. (a) Ultrathin LBL films formed from alternating layers of PANI/PVS on a PS substrate; (b) Representation of the PANI/PVS films and (c) a parallel pair of printed electrodes (thickness of $\sim 3 \mu\text{m}$, length (X) of 10 mm and distance (L) of 600 μm). (d) Mechanical cutting process to (e) establish a single sensor (area of 0.5 cm^2); (f) Image of ammonia gas sensors using ultrathin PANI/PVS films on the PS substrate.

for the complex impedance measurements using the same procedure as described elsewhere^[13].

Finally, to confirm the reproducibility, stability, and operating range of the sensor, repeated ten cycles of electrical measurements were made using three films from the same batch.

3. Results and Discussions

Figure 2 shows the multilayer film growth and morphological characterization of the PANI/PVS ultrathin films grown by LBL deposition on the PS substrate from 0 to 25 bilayers (n). UV-Vis absorption spectroscopy (Figure 2a) showed that the multilayer LBL films can be grown in a controlled way in terms of thickness at the nanometre scale, indicating that the same amount of material was adsorbed in each deposition step^[30]. The inset in Figure 2a shows the linear dependence of the PANI/PVS thickness on n . This linear dependence was obtained from the UV-Vis absorption spectra at 900 nm. Figure 2b shows the AFM images obtained from n equal to 0, 1, 15, and 25. For n varying from 1 to 15, the AFM images suggest that the film growth results from PANI/PVS particles' nucleation on the surface, where the height growth rate is higher compared to their growth laterally. However, a transition is observed in film grown at $n \sim 15$. In this case, when n varies from 15 to 25, the lateral growth rate is higher compared to their growth in height. For $n \geq 15$, this result suggests that the morphology of PANI/PVS on PS varied from a rod-like structure to a film-like architecture, becoming more uniform gradually thickness-homogeneous films for a further improvement in device performance over n to obtain. This rod-like to film-like transition is consistent with the previous studies of Santos et al.^[31] and Lobo et al.^[32], where 25 bilayers of PANI/PVS films on a glass substrate were more homogeneous than films with $n < 15$, resulting in a smooth surface morphology, which is highly desirable to ensure a uniform electrical field distribution along with the polymer sensor. Furthermore, the advantage of the architecture over the rod structure for device performance is important to optimize the performance of the semiconductor thin film by the density of hopping carriers proportionally with n . This growth process is represented in Figure 2c, where the evolution of UV-Vis absorption at 900 nm and average roughness of PANI/PVS shows a behavior transition at $n = 15$ ^[31]. The self-nucleation of PANI/PVS particles is represented in Figure 2d with increasing bilayers in the PS substrate to which linear fitting obtained corresponds (4.8 ± 0.6).

Figure 3 shows how the $Z'(f)$ and $Z''(f)$ components (Bode and Nyquist plots) of the flexible PANI/PVS-based sensors vary with n from 5 to 25 (Figure 3a), and also for $n = 25$ varying the ammonia gas concentration (Figure 3b) and strain (Figure 3c) from 0 to 25 ppm and from 0 to 25%, respectively. According to Lobo et al.^[32], in the LBL technique the increase in the number of bilayers results from by compaction of the semiconductor polymer molecules. The result in Figure 3a demonstrates that the molecular aggregation favors the reduction of the value of $Z'(f)$ from dc regime ($f \rightarrow 0$) which would increase electrical conductivity. Therefore, we choose $n = 25$ to investigate

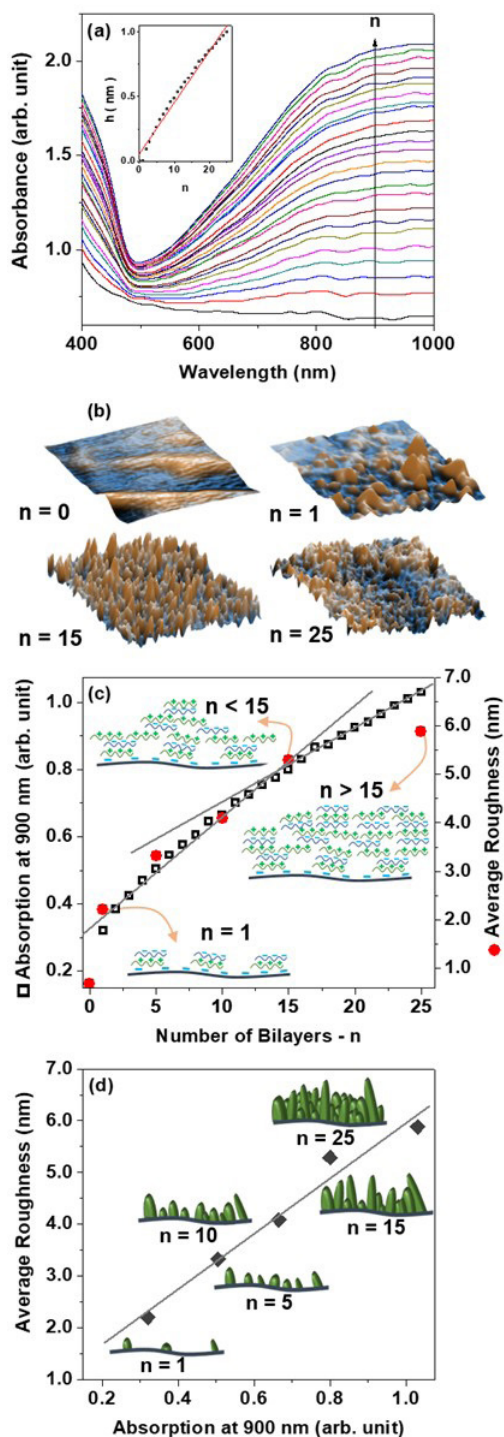


Figure 2. Multilayer film growth and morphological characterisation of PANI/PVS ultrathin films grown by LBL deposition on the PS substrate. (a) UV-Vis absorption spectra of PANI/PVS films for $n = 1-25$. The inset shows the linear dependence of PANI/PVS thickness on n ; (b) AFM images ($2.5 \times 2.5 \mu\text{m}^2$) of n onto PS substrate; (c) UV-Vis absorption at 900 nm and the average roughness according to n , showing a schematic representation of the growth transition at $n \sim 15$; (d) Linear correlation of PANI absorption at 900 nm and average roughness associated with the PANI/PVS growth mechanism changing from a rod-like structure ($n < 15$) to a film-like architecture ($n \geq 15$).

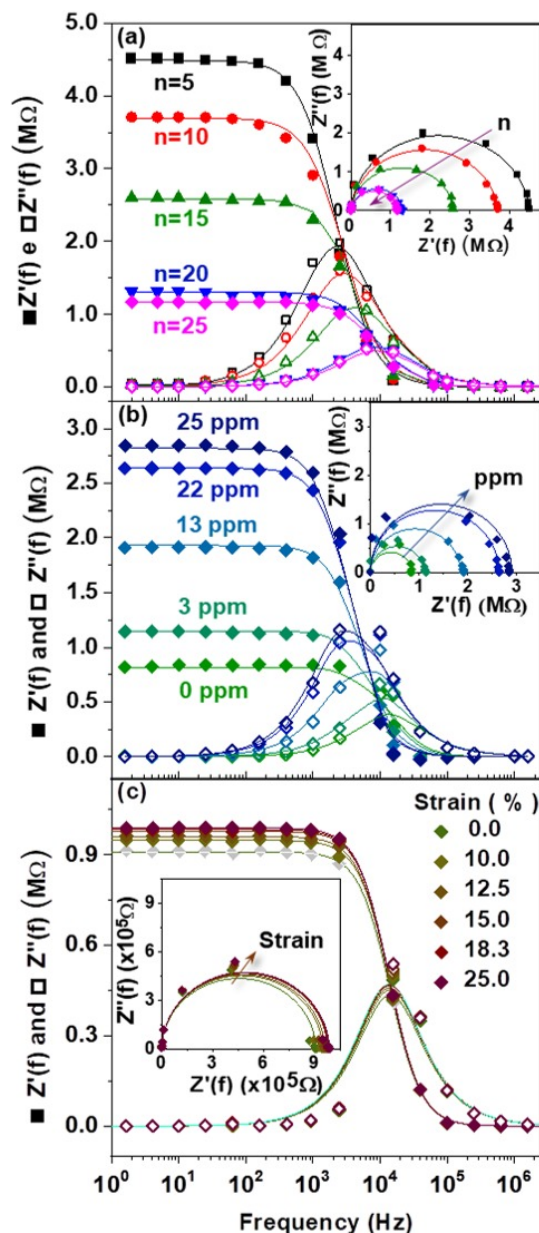


Figure 3. Real, $Z'(f)$, and imaginary, $Z''(f)$, components of the complex impedance, Argand diagram [$Z'(f)$ vs. $Z''(f)$] and the experimental-theoretical fittings using the Cole-Cole model represented by the full lines. (a) PANI/PVS films with n from 5 to 25. The inset shows an illustration of a Ag electrode pair and its contact area with the film; (b) A PANI/PVS flexible device (made from 25 bilayers of PANI/PVS) exposed to 0, 3, 13, 22 and 25 ppm of ammonia gas levels; (c) PANI/PVS flexible device under tensile stress varying the initial length from 0 to 3 mm. The inset shows the PANI/PVS device with initial length L_0 and under stress T with varying the length L_1 (0–3 mm).

device performance under ammonia to guarantee a film-like architecture for the PANI/PVS films.

Figure 3 shows the quasi-Debye dispersion patterns to all $Z'(f)$ and $Z''(f)$. These behaviours allow the representation of complex impedance by the Cole-Cole relaxation model,

Equation 1, in which a parallel resistor-capacitor circuit to model the store/dissipated charge effects is used to represent the symmetric parameter ($0 < \alpha < 1$) related to the relaxation peaks of the PANI/PVS films^[13].

$$Z^*(f) = R / [1 + (i2\pi fRC)^\alpha] \quad (1)$$

Table 1 shows the parameters obtained from the fitting of $Z'(f)$ and $Z''(f)$ using Equation 1) for a flexible PANI/PVS-based sensor for different n values, ammonia concentrations ([NH₃]) and strain values. The results show that the electrical resistance (R) of the PANI/PVS films decreases with n and increases with ammonia concentration and strain. At the same time, the capacitance (≈ 10 -11 F) and the parameter ($\alpha = 0.99$) are almost independent of n , [NH₃], and strain. The $\alpha < 1$ and the dielectric constant $k \approx 105$, obtained by $C = \epsilon_0 \epsilon Xh/L$ (using $X = 10$ mm), $h = 100$ nm for $n = 25$ and $L = 600$ μ m), supporting the establishment of mesoscopic metallic regions from the increasing percent crystallinity, the size of crystalline regions, and/or polymer chain alignment in the disordered regions of PANI-based films^[33]. This is in good agreement with ref^[30]. Moreover, the value of k is typical of PANI^[32], and $Z'(f) = R$ in the 1 to 100 Hz frequency range, the sensibility of the sensor for n , [NH₃], and strain are ~ 1.8 M Ω /unit, 98 k Ω /ppm, and 3.6 k Ω %, respectively.

From Figure 4, we can observe the linear variation of normalized resistance (R/R_0) obtained from the fittings of $Z'(f)$ and $Z''(f)$ using Equation 1 as a function of n (Figure 4a), [NH₃] (Figure 4b) and strain (Figure 4c). In this figure, R_0 is the resistance value obtained when $n = 5$, [NH₃] = 0 ppm and zero strain. Taken together, these findings highlight that the PANI/PVS films act as a resistive sensor for ammonia in which the operating frequency range is 1 to 100 Hz and show low strain sensing behavior, thereby fulfilling the requirements

Table 1. Data for fitting using Equation 1 for samples with different n , doping (ppm) and tensile stress (%) varying from 5 to 25 bilayers, 0 to 25 ppm and 0 to 25%, respectively. The parameter $\alpha = 0.99$ was obtained for all experimental-theoretical fittings.

	n (unit)	R (M Ω)	C (10 ⁻¹¹ F)
[NH ₃]=0 Strain = 0	5	4.49	1.50
	10	3.70	1.45
	15	2.59	1.44
	20	1.31	1.41
	25	1.17	1.39
$n = 25$ [NH ₃] (ppm)	0	0.85	1.40
	3	1.10	1.43
	13	1.85	1.46
	22	2.64	1.49
	25	2.90	1.51
$n = 25$ [NH ₃] = 0 Strain (%)	0	0.91	1.24
	12	0.95	1.20
	15	0.97	1.19
	18	0.98	1.17
	25	0.99	1.16

for a flexible ammonia sensor with high mechanical stability. In this figure, S is the sensitivity coefficient of the device for n ($S = 0.6 \pm 0.3$ M Ω /n), [NH₃] ($S = 98 \pm 2$ k Ω /ppm) and strain ($S = 3.6 \pm 0.5$ k Ω /%).

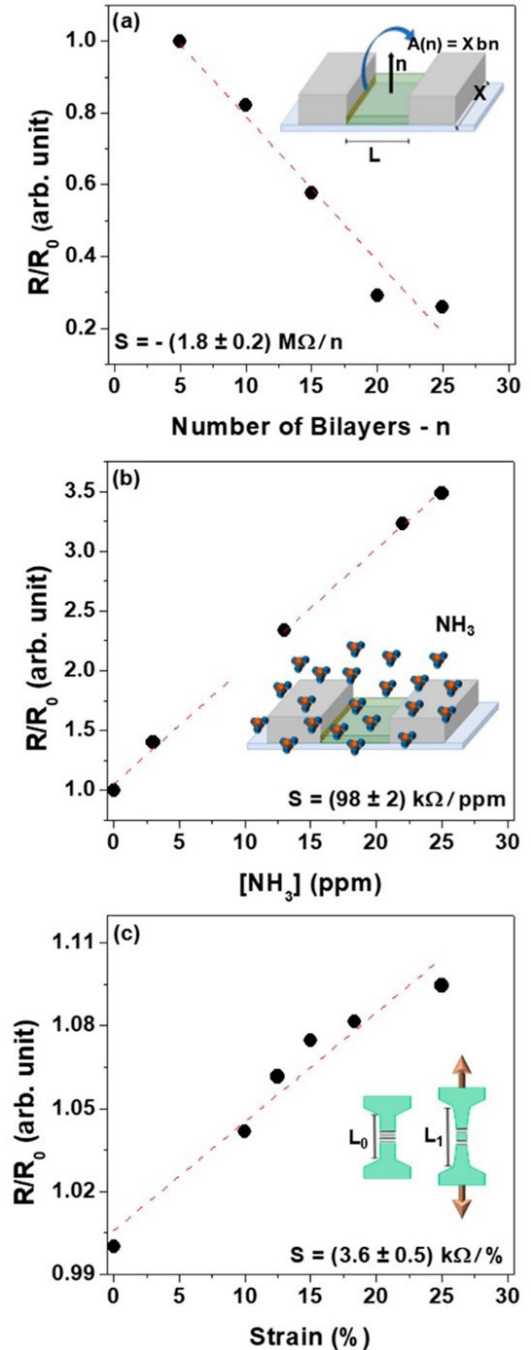


Figure 4. Sensitivity of flexible PANI/PVS devices by correlating the electrical resistance quotient using the initial value R/R_0 and (a) $n = 0$ -25; (b) the ammonia gas concentration level ranging from 0 to 25 ppm and (c) the stretching of the flexible PANI/PVS devices ranging from 0 to 25% of the initial size L_0 . The standard error of the curves $\sim 20\%$.

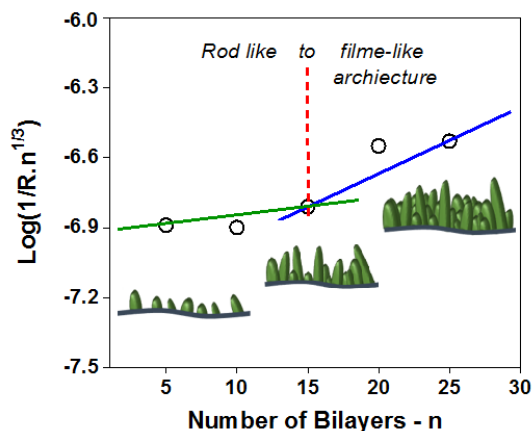


Figure 5. Log $1/(R.n^{1/3})$ vs. $n^{1/3}$ using Equation 2 and the parameters R and n from Table 1. Standard error for $5 \leq n \leq 15$ and of $15 \leq n \leq 25$ regions are lower than 10 %.

For the study of the conduction process of ultrathin PANI/PVS sensors, we assume that the admittance ($1/R$) is directly proportional to both electrical current and the nucleation of PANI/PVS particles induced by n (or the film growth) through the electronic hopping process described^[25,33-35], and in agreement with both the establishment of mesoscopic metallic regions (conductive islands)^[33] and the AFM results shown in Figure 2b. For this case, we expected the following dependence of the dc conductivity, represented here by $1/Rn^{1/3}$ and that the concentration of hopping carriers remains constant independent of n ^[25,34] according to the expression:

$$\text{Log}\left[1/(Rn^{1/3}) \approx n^{1/3}\right] \quad (2)$$

It indicates that the mobility of hopping carriers may change with the number of bilayers, while the concentration of hopping carriers remains constant. These effects are similar to those observed due to the doping level in polyaniline^[32].

Figure 5 shows the Log $1/(R.n^{1/3})$ vs. n curve obtained through Equation 2. From the results shown in Figure 5, it is concluded that the mobility of hopping carriers changes with n . In contrast, the concentration of hopping carriers remains constant, as expected for moderately doped PANI^[25,33,34]. Furthermore, $n = 15$ represents a region of rod-like transition to film-like architecture, as seen in Figure 2b.

In this equation, ω is the angular frequency obtained by $\omega = 2\pi f$, R is the dc electrical resistance, C is the electrical capacitance, and α is a parameter of dielectric relaxation that can assume values between 0 and 1; this shows that the distribution of relaxation times was highly.

4. Conclusions

We have explored the AC electrical, morphological, and mechanical behavior of ultrathin PANI/PVS films by combining AC, morphology, ammonia concentration and tensile stress-strain measurements for improving flexible device performance. We employed the complex impedance technique for the proper adjustment of the

operating frequency of the device. This approach has the potential features to effectively distinguish the resistive and capacitive contributions of the PANI-based sensor in a wide frequency range. Consequently, it establishes an operating frequency range from 10 to 100 Hz and response time (< 1 min) of the solution-processed sensor. The empirical Cole-Cole relaxation function was chosen to investigate the ultrathin polymer film-based flexible films. The Cole-Cole dielectric response provided the same dielectric parameter ($\alpha < 1$) to all cases. This suggests that the distribution of the circuit elements on the bulk of the material is almost homogeneous. The distribution of relaxation times depends on the LBL process, the chemical doping, or the mechanical deformation. Meanwhile, the surface morphology varies from a rod-like structure to a film-like architecture, and the mobility of hopping carriers changes with n while the concentration of hopping carriers remains constant. The uniform and homogeneous surface of PANI/PVS films improve device performance avoiding electrode effects, as shown in ref.^[30] and the rod-like structure. Finally, our study provides an extensive analysis of polymer-based flexible devices from impedance spectroscopy measurements in a wide frequency range. Our results demonstrated that PANI/PVS ultra-thin films have electrical sensitivity for mechanical strain varying from 0 to 25%. In addition to all this, it highlights the importance of simultaneously exploring the morphology and complex impedance measurements to provide a powerful methodology for enhancing polymers' electrical performance for sensor technology development.

5. Author's Contribution

- **Conceptualization** – Rodrigo Fernando Bianchi; Ana Carolina Kelmer; Cleidinéia Cavalcante da Costa.
- **Data curation** – Rodrigo Fernando Bianchi; Ana Carolina Kelmer; Cleidinéia Cavalcante da Costa.
- **Formal analysis** – Rodrigo Fernando Bianchi; Ana Carolina Kelmer.
- **Funding acquisition** – Rodrigo Fernando Bianchi.
- **Investigation** – Rodrigo Fernando Bianchi; Ana Carolina Kelmer; Cleidinéia Cavalcante da Costa.
- **Methodology** – Rodrigo Fernando Bianchi; Ana Carolina Kelmer; Cleidinéia Cavalcante da Costa.
- **Project administration** – Rodrigo Fernando Bianchi; Ana Carolina Kelmer; Cleidinéia Cavalcante da Costa.
- **Resources** – Rodrigo Fernando Bianchi; Ana Carolina Kelmer; Cleidinéia Cavalcante da Costa.
- **Software** – Rodrigo Fernando Bianchi; Ana Carolina Kelmer; Cleidinéia Cavalcante da Costa.
- **Supervision** – Rodrigo Fernando Bianchi.
- **Validation** – Rodrigo Fernando Bianchi; Ana Carolina Kelmer; Cleidinéia Cavalcante da Costa.
- **Visualization** – Rodrigo Fernando Bianchi; Ana Carolina Kelmer; Cleidinéia Cavalcante da Costa.
- **Writing – original draft** – Rodrigo Fernando Bianchi; Ana Carolina Kelmer; Cleidinéia Cavalcante da Costa.

• **Writing – review & editing** – Rodrigo Fernando Bianchi; Ana Carolina Kelmer; Cleidinéia Cavalcante da Costa.

6. Acknowledgements

This work was supported by INEO, FAPEMIG (APQ-03165-17), CNPq (308185/2016-1) and CAPES (001).

7. References

- Zhang, D., Huang, T., & Duan, L. (2020). Emerging self-emissive technologies for flexible displays. *Advanced Materials*, 32(15), 1902391. <http://dx.doi.org/10.1002/adma.201902391>. PMID:31595613.
- Wang, L., Lou, Z., Jiang, K., & Shen, G. (2019). Bio-multifunctional smart wearable sensors for medical devices. *Advanced Intelligent Systems*, 1(5), 1900040. <http://dx.doi.org/10.1002/aisy.201900040>.
- Feng, S., Farha, F., Li, Q., Wan, Y., Xu, Y., Zhang, T., & Ning, H. (2019). Review on smart gas sensing technology. *Sensors (Basel)*, 19(17), 3760. <http://dx.doi.org/10.3390/s19173760>. PMID:31480359.
- Wang, Y., Liu, A., Han, Y., & Li, T. (2020). Sensors based on conductive polymers and their composites: a review. *Polymer International*, 69(1), 7-17. <http://dx.doi.org/10.1002/pi.5907>.
- Bandodkar, A. J., Jeerapan, I., & Wang, J. (2016). Wearable chemical sensors: present challenges and future prospects. *ACS Sensors*, 1(5), 464-482. <http://dx.doi.org/10.1021/acssensors.6b00250>.
- Hussain, A. M., Ghoneim, M. T., Rojas, J. P., & Fahad, H. (2019). Flexible and/or stretchable sensor systems. *Journal of Sensors*, 2019, 1828394. <http://dx.doi.org/10.1155/2019/1828394>.
- Dahiya, R., Yogeswaran, N., Liu, F., Manjakkal, L., Burdet, E., Hayward, V., & Jorntell, H. (2019). Large-area soft e-skin: the challenges beyond sensor designs. *Proceedings of the IEEE*, 107(10), 2016-2033. <http://dx.doi.org/10.1109/JPROC.2019.2941366>.
- Kumar, K. S., Chen, P.-Y., & Ren, H. (2019). A review of printable flexible and stretchable tactile sensors. *Research*, 2019, 3018568. <http://dx.doi.org/10.34133/2019/3018568>.
- Bach-Toledo, L., Hryniewicz, B. M., Marchesi, L. F., Dall'Antonia, L. H., Vidotti, M., & Wolfart, F. (2020). Conducting polymers and composites nanowires for energy devices: a brief review. *Materials Science for Energy Technologies*, 3, 78-90. <http://dx.doi.org/10.1016/j.mset.2019.09.006>.
- Haneef, H. F., Zeidell, A. M., & Jurchescu, O. D. (2020). Charge carrier traps in organic semiconductors: a review on the underlying physics and impact on electronic devices. *Journal of Materials Chemistry. C, Materials for Optical and Electronic Devices*, 8(3), 759-787. <http://dx.doi.org/10.1039/C9TC05695E>.
- McBride, M., Liu, A., Reichmanis, E., & Grover, M. A. (2020). Toward data-enabled process optimization of deformable electronic polymer-based devices. *Current Opinion in Chemical Engineering*, 27, 72-80. <http://dx.doi.org/10.1016/j.coche.2019.11.009>.
- Mapa, L. M., Golin, A. F., Costa, C. C., & Bianchi, R. F. (2019). The use of complex impedance spectroscopy measurements for improving strain sensor performance. *Sensors and Actuators. A, Physical*, 293, 101-107. <http://dx.doi.org/10.1016/j.sna.2019.02.001>.
- Santos, M. C., Hamdan, O. H. C., Valverde, S. A., Guerra, E. M., & Bianchi, R. F. (2019). Synthesis and characterization of v2o5/pani thin films for application in amperometric ammonia gas sensors. *Organic Electronics*, 65, 116-120. <http://dx.doi.org/10.1016/j.orgel.2018.11.013>.
- Alrammouz, R., Podlecki, J., Abboud, P., Sorli, B., & Habchi, R. (2018). A review on flexible gas sensors: from materials to devices. *Sensors and Actuators. A, Physical*, 284, 209-231. <http://dx.doi.org/10.1016/j.sna.2018.10.036>.
- Zhang, W., Wu, Z., Hu, J., Cao, Y., Guo, J., Long, M., Duan, H., & Jia, D. (2020). Flexible chemiresistive sensor of polyaniline coated filter paper prepared by spraying for fast and non-contact detection of nitroaromatic explosives. *Sensors and Actuators. B, Chemical*, 304, 127233. <http://dx.doi.org/10.1016/j.snb.2019.127233>.
- Fratoddi, I., Venditti, I., Cametti, C., & Russo, M. V. (2015). Chemiresistive polyaniline-based gas sensors: a mini review. *Sensors and Actuators. B, Chemical*, 220, 534-548. <http://dx.doi.org/10.1016/j.snb.2015.05.107>.
- Nagare, A. B., Harale, N. S., Mali, S. S., Nikam, S. S., Patil, P. S., Hong, C. K., & Moholkar, A. V. (2019). Chemiresistive ammonia gas sensor based on branched nanofibrous polyaniline thin films. *Journal of Materials Science Materials in Electronics*, 30(13), 11878-11887. <http://dx.doi.org/10.1007/s10854-019-01514-7>.
- Zhang, T., Qi, H., Liao, Z., Horev, Y. D., Panes-Ruiz, L. A., Petkov, P. S., Zhang, Z., Shivhare, R., Zhang, P., Liu, K., Bezugly, V., Liu, S., Zheng, Z., Mannsfeld, S., Heine, T., Cuniberti, G., Haick, H., Zschech, E., Kaiser, U., Dong, R., & Feng, X. (2019). Engineering crystalline quasi-two-dimensional polyaniline thin film with enhanced electrical and chemiresistive sensing performances. *Nature Communications*, 10(1), 4225. <http://dx.doi.org/10.1038/s41467-019-11921-3>. PMID:31548543.
- Song, E., & Choi, J.-W. (2013). Conducting polyaniline nanowire and its applications in chemiresistive sensing. *Nanomaterials (Basel, Switzerland)*, 3(3), 498-523. <http://dx.doi.org/10.3390/nano3030498>. PMID:28348347.
- Souza, N. C., Silva, J. R., Pereira-Da-Silva, M. A., Raposo, M., Faria, R. M., Giacometti, J. A., & Oliveira, O. N. (2004). Dynamic scale theory for characterizing surface morphology of layer-by-layer films of poly(o-Methoxyaniline). *Journal of Nanoscience and Nanotechnology*, 4(5), 548-552. <http://dx.doi.org/10.1166/jnn.2004.084>. PMID:15503441.
- Bao, Q., Braun, S., Wang, C., Liu, X., & Fahlman, M. (2019). Interfaces of (Ultra)thin polymer films in organic electronics. *Advanced Materials Interfaces*, 6(1), 1800897. <http://dx.doi.org/10.1002/admi.201800897>.
- Ramgir, N. S. (2013). Electronic nose based on nanomaterials: issues, challenges, and prospects. *ISRN Nanomaterials*, 2013, 941581. <http://dx.doi.org/10.1155/2013/941581>.
- Couto, J. D., Santos, M. C., & Bianchi, R. F. (2019). Exploring the universality of the alternating conductivity of disordered materials using gaussian distribution of activation energies. *Materials Research Express*, 6(4), 046302. <http://dx.doi.org/10.1088/2053-1591/aad1ce>.
- Wong, Y. C., Ang, B. C., Haseeb, A. S. M. A., Baharuddin, A. A., & Wong, Y. H. (2020). Conducting polymers as chemiresistive gas sensing materials: a review. *Journal of the Electrochemical Society*, 167(3), 037503. <http://dx.doi.org/10.1149/2.0032003JES>.
- Calheiro, D. S., & Bianchi, R. F. (2019). Tuning the detection limit in hybrid organic-inorganic materials for improving electrical performance of sensing devices. *Sensors and Actuators. A, Physical*, 298, 111480. <http://dx.doi.org/10.1016/j.sna.2019.07.005>.
- Santos, M. C., Bianchi, A. G. C., Ushizima, D. M., Pavinatto, F. J., & Bianchi, R. F. (2017). Ammonia gas sensor based on the frequency-dependent impedance characteristics of ultrathin

- polyaniline films. *Sensors and Actuators. A, Physical*, 253, 156-164. <http://dx.doi.org/10.1016/j.sna.2016.08.005>.
27. Diniz, M. O., Golin, A. F., Santos, M. C., Bianchi, R. F., & Guerra, E. M. (2019). Improving performance of polymer-based ammonia gas sensor using POMA/V2O5 hybrid films. *Organic Electronics*, 67, 215-221. <http://dx.doi.org/10.1016/j.orgel.2019.01.039>.
 28. Faria, A. M. A., Miranda, M. A., Gonçalves, G. E., Bianchi, R. F., Bianchi, A. G. C., Cuba, C., Neves, B. R. A., & Pinto, E. S. (2020). Partially ordered porous structures on layer-by-layer Polyaniline/Poly(Vinyl Sulfate Sodium) ultrathin films: easy fabrication of robust submicroscopic patterning. *Journal of Applied Polymer Science*, 137(17), 48597. <http://dx.doi.org/10.1002/app.48597>.
 29. Santos, M. C., Santos, F. A., Teixeira, F. P., Gonçalves, G. E., Bianchi, A. G. C., & Bianchi, R. F. (2007). Caracterização elétrica de filmes ultrafinos de PANI/PVS: material potencial para detecção de amônia em galpões de criação avícola. *Polímeros: Ciência e Tecnologia*, 20(3), 107-111. <http://dx.doi.org/10.1590/S0104-14282010005000018>.
 30. Ferreira, M., Fiorito, P. A., Oliveira, O. N., Jr., & Torresi, S. I. C. (2004). Enzyme-mediated amperometric biosensors prepared with the Layer-by-Layer (LbL) adsorption technique. *Biosensors & Bioelectronics*, 19(12), 1611-1615. <http://dx.doi.org/10.1016/j.bios.2003.12.025>. PMID:15142594.
 31. Santos, M. C., Munford, M. L., & Bianchi, R. F. (2012). Influence of NiCr/Au electrodes and multilayer thickness on the electrical properties of PANI/PVS ultrathin film grown by LbL deposition. *Materials Science and Engineering B*, 177(4), 359-366. <http://dx.doi.org/10.1016/j.mseb.2011.12.039>.
 32. Lobo, R. F. M., Pereira-da-Silva, M. A., Raposo, M., Faria, R. M., & Oliveira, O. N., Jr. (2003). The morphology of layer-by-layer films of Polymer/Polyelectrolyte studied by atomic force microscopy. *Nanotechnology*, 14(1), 101-108. <http://dx.doi.org/10.1088/0957-4484/14/1/322>.
 33. Bianchi, R. F., Ferreira, G. F. L., Lepienski, C. M., & Faria, R. M. (1999). Alternating electrical conductivity of polyaniline. *The Journal of Chemical Physics*, 110(9), 4602-4607. <http://dx.doi.org/10.1063/1.478341>.
 34. Neto, J. M. G., Ferreira, G. F. L., Santos, J. R., Jr., Cunha, H. N., Dantas, I. F., & Bianchi, R. F. (2003). Complex conductance of Carnauba Wax/Polyaniline composites II experimental procedure experimental results. *Brazilian Journal of Physics*, 33(2), 371-375. <http://dx.doi.org/10.1590/S0103-97332003000200040>.
 35. Bianchi, R. F., Cunha, H. N., Faria, R. M., Ferreira, G. F. L., & Neto, J. M. G. (2005). Electrical studies on the doping dependence and electrode effect of Metal-PANI-Metal structures. *Journal of Physics. D, Applied Physics*, 38(9), 1437-1443. <http://dx.doi.org/10.1088/0022-3727/38/9/017>.

Received: Aug. 01, 2023

Revised: Nov. 05, 2023

Accepted: Jan. 07, 2024